Published online 16 December 2012 *Nucleic Acids Research, 2013, Vol. 41, No. 3* **2009–2019**
doi:10.1093/nar/gks1206

Magnetic tweezers measurements of the nanomechanical stability of DNA against denaturation at various conditions of pH and ionic strength

Alessia Tempestini[1], Valeria Cassina[1], Doriano Brogioli[1], Roberto Ziano[1], Simona Erba[1], Roberto Giovannoni[2], Maria G. Cerrito[2], Domenico Salerno[1,*] and Francesco Mantegazza[1]

[1]Dipartimento di Scienze della Salute, Università di Milano-Bicocca, via Cadore 48, Monza (MB) 20900, Italy and [2]Dipartimento di Chirurgia e Medicina Interdisciplinare, Università di Milano-Bicocca, via Cadore 48, Monza (MB) 20900, Italy

Received July 25, 2011; Revised October 25, 2012; Accepted October 30, 2012

ABSTRACT

The opening of DNA double strands is extremely relevant to several biological functions, such as replication and transcription or binding of specific proteins. Such opening phenomenon is particularly sensitive to the aqueous solvent conditions in which the DNA molecule is dispersed, as it can be observed by considering the classical dependence of DNA melting temperature on pH and salt concentration. In the present work, we report a single-molecule study of the stability of DNA against denaturation when subjected to changes in solvent. We investigated the appearance of DNA instability under specific external applied force and imposed twist values, which was revealed by an increase in the temporal fluctuations in the DNA extension. These fluctuations occur in the presence of a continuous interval of equilibrium states, ranging from a plectonemic state to a state characterized by denaturation bubbles. In particular, we observe the fluctuations only around a characteristic force value. Moreover, this characteristic force is demonstrated to be notably sensitive to variations in the pH and ionic strength. Finally, an extension of a theoretical model of plectoneme formation is used to estimate the average denaturation energy, which is found to be linearly correlated to the melting temperature of the DNA double strands.

INTRODUCTION

DNA denaturation is at the origin of many biological phenomena, for example, replication, transcription and the interaction of specific proteins with single-stranded DNA. In the present work, we conducted a direct quantitative characterization of DNA denaturation at the single-molecule level. Given the influence of environmental conditions on the biological activity of DNA, we performed measurements in different conditions of pH and ionic strength.

Single-molecule techniques are particularly relevant in the current panorama of biophysical research because they have opened new roads to the analysis of several biological and biomedical problems that are not easily observable with ensemble measurements (1–3). Typical examples of single molecule techniques are magnetic tweezers (MT) (4–8), optical tweezers (9–12), atomic force microscopy (13–16) and single-molecule fluorescence spectroscopy (17,18). Compared with the other techniques, MT methods have a straightforward implementation, and given their capability for applying torsional constrain, MT allows the study of single molecules in conditions that are not easily accessible with the other methods (19,20). Recently, valuable torsional experiments have also been performed with optical tweezers with unconventional nanoparticles (21–23) or by exploiting refined analysis (20,24), but MT nanomanipulation still offers a simpler strategy for applying force and twist to single molecules.

The MT technique is based on the manipulation of a single DNA molecule linked to magnetic spherical

*To whom correspondence should be addressed. Tel: +39 02 6448 8215; Fax: +39 02 6448 8068; Email: domenico.salerno@unimib.it

The authors wish it to be known that, in their opinion, the first two authors should be regarded as joint First Authors.

microparticles by means of external magnetic fields (6). The microparticles are suspended in water solutions, but they are not freely diffusing because they are connected to the inner walls of a capillary tube by single DNA molecules. Force and twist are applied to the bead through a field generated by external permanent magnets or electromagnets. The movement of the bead is transferred to the sample, and thus force and twist are applied to the DNA.

The first MT studies addressed the topology of individual DNA molecules by measuring DNA extension as a function of the applied force and imposed torsion (25–27). In particular, it was observed that DNA extension is influenced by torsion producing plectonemes (28). In certain conditions of torsional stress at high forces, MT nanomanipulation can also induce a denaturation, which is obtained only with the negative torsion because of the chirality and natural helical orientation DNA (4). In the present work, we show the results of a series of MT experiments, where we evaluated the dependence of the stability of double-strand DNA, that is, denaturation bubbles (29–33), DNA breathing (34) or DNA melting (35,36), on the imposed turns and applied force. The experiments were performed with DNA in standard phosphate buffered saline (PBS) at pH 7.4 and at various pH values and ionic strengths. The results are particularly interesting because DNA stability influences a host of biological functions, such as DNA binding with transcription machinery and the replication process (37–39). It should be observed that the energy landscape of the denaturation-plectoneme transition was recently analysed in (40), and in the present article, we extend those results probing explicitly the effects of pH and ionic strength. Furthermore, other articles discussed the DNA phase diagram in the force–torsion space (35). Here, we concentrate on the plectonemic-denaturation transition, in the force-turns space, never explored before.

MATERIALS AND METHODS

Capillary flow cell preparation

The capillary flow cell (1×1 mm^2 section, 5 cm long, VitroCom, Mountain Lakes, NJ, USA) was prepared according to a method in the literature (41). Briefly, the internal walls were uniformly coated with polystyrene (average molecular weight = 230 000, Aldrich, Milan, Italy) (42) and were coated with 5 µg of sheep polyclonal anti-digoxigenin antibody (Roche, Milan, Italy). The treated surface was passivated for 2 h at 37°C with a solution consisting of PBS pH 7.4, 0.1% of Tween-20, 10 mg/ml of bovine serum albumin (Roche) and 3 mM of NaN_3 (4).

DNA and magnetic bead preparation

The DNA molecule required to perform an MT experiment must be bound at one end to an immobile support (the glass capillary) and at the other end to a magnetic bead (5). The DNA molecule used in this work was 7000 bp long and was assembled by a central part extracted from pCMV6-Neo plasmid (5780 bp, ~1.9 µm) and by two functionalized ends. One end was modified by digoxigenin, and the other end was modified with biotin to provide a connection to the immobile support (the anti-digoxigenin-coated capillary) and to the mobile support (the avidin-coated magnetic bead), respectively. Following the methods previously reported in the literature (6), the DNA tails were functionalized by polymerase chain reaction; thus, the DNA was attached via multiple bonds to the supports. The molecule results torsionally constrained so that the rotation of the magnets induces a real torque on the DNA, which could not swivel around the bonds. As it was already reported (6), we used 1-µm diameter, streptavidin-coated, superparamagnetic beads (Dynabeads MyOne Streptavidin C1, Dynal, Invitrogen, Milan, Italy). We added 1 µl of the bead solution to 10 µl of the functionalized DNA solution for a final concentration of 1×10^6 molecules of DNA per microlitres. After 5 min of incubation, the DNA + microbeads solution was diluted in 500 µl of PBS pH 7.4, supplemented with 0.1% of Tween-20 and 3 mM of NaN_3 (referred to hereafter as PBS–Tween-20); the solution was subsequently injected into the capillary. Finally, after 1 h of incubation, we washed out all of the unattached beads with a solution of PBS–Tween-20 pH 7.4.

pH and ionic strength characterization

To study the influence of environmental conditions, DNA properties were analysed in solutions having different pH and ionic strength values from those of the standard PBS at pH 7.4. The PBS solutions for measurement in different pH conditions were prepared by balancing Na_2HPO_4 and KH_2PO_4 to obtain different values of pH and by changing the NaCl concentration to maintain constant ionic strength. The resulting values of pH were checked by a standard pHmeter (Mettler Toledo, Milan, Italy). The range of pH explored was $5 < pH < 9$.

The PBS solutions for measurement in different ionic strength conditions were prepared by modifying only the NaCl concentration (5, 50, 150, 395 and 500 mM) and maintaining the pH at 7.4. The resulting conductivity of the solution was checked by a conductimeter. For measurements at different conditions, at least 10 volumes of the solution was injected into the capillary to ensure complete substitution of the buffer.

MT technique

Our MT apparatus followed the most classical proposed schemes (5–7), and it has been previously described elsewhere (41,43,44). The capillary, which is linked to a buffer-flow system, is placed over a homemade inverted microscope, which is composed of an objective (Nikon 100×, 1.25-NA oil immersion with a 15-cm focal-length tube lens leading to an actual magnification of 75×) and is equipped with a piezoelectric focusing system (PIFoc, Physik Instrumente, Bresso, Italy). Images were acquired at a rate of 60 frames per second with a Charge-Coupled Device (CCD) camera (Marlin, Allied Vision Technologies) and were fed into a Personal Computer.

Data analysis

By considering the diffraction images generated at different heights of the bead, illuminated by a light emitting diode (LED) light (45,46), the DNA extension was calculated. A force is exerted (by the magnetic field of the external magnets) on the bead and consequently also on the DNA; the force was measured from the x–y fluctuations of the bead, as previously described (7,8). The mean square displacement $\sigma_x^2 = \langle (x - \langle x \rangle)^2 \rangle$ was evaluated with an appropriate correction for the camera integration time (8,41,47). Next, we extracted the force F with the equipartition theorem (4,7): $F = k_B \cdot T \cdot L_e / \sigma_x^2$, where k_B is the Boltzmann constant, T is the temperature and L_e is the DNA extension. Once the applied force was calibrated in this manner, we were able to apply a known force to the bead. In the explored regime, the DNA extension L_e is an increasing function of the applied force F and the specific dependence of L_e versus F can be interpreted in the framework of the so-called worm-like chain model (48). By simply rotating the external magnets at a fixed height (and thus at a fixed applied force), we can apply a twist to the torsionally constrained DNA molecule.

RESULTS

We have measured the average extension $\langle L_e \rangle$ of a DNA molecule as a function of the number of imposed turns n_t or analogously as a function of the degree of supercoiling $\sigma = \frac{\Delta L_k}{L_{k0}}$ (L_{k0} is the natural linking number in absence of external constraints, and ΔL_k is the excess or deficit of L_k). The obtained data are shown in Figure 1 (upper panel) for the classical representative case of DNA at standard conditions (pH = 7.4, ionic strength I_s = 150 mM) and for two different values of the applied pulling force (F = 1.2 and 0.45 pN). The mean value $\langle L_e \rangle$ was obtained by averaging over a time interval of several seconds, as detailed later. The circular labels A, B, C and D located on the data of Figure 1 (upper panel) correspond to the sketches of Figure 1A–D (lower panels), which provide an idea of the actual behaviour of DNA under the actions of torsion and force. As previously described in literature (6) and visually depicted by the sketches of Figure 1, the effects of applied force and imposed twist are as follows: forming a plectoneme (Figure 1C), extending the DNA (Figure 1A and B) and forming a denaturation bubble (Figure 1D). There are detailed experimental studies of the initial stages of plectoneme formation and rigorous nanomechanical models of the buckling and post-buckling behaviour of chains under torsion (49–53). However, we believe that our naïve sketches are still valuable and describe the primary characteristics of the experimental findings.

The $\langle L_e \rangle$ as a function of n_t data are presented in Figure 2 for certain values of the applied pulling force (F = 1.2 pN, F = 0.8 pN and F = 0.5 pN). The results correspond to those of the classical MT literature (6). In this study, we concentrated our attention on the temporal statistical fluctuations of the data and particularly on the standard deviation σ_{L_e} of the DNA extension measurements. The histograms in the insets of Figure 2 show the

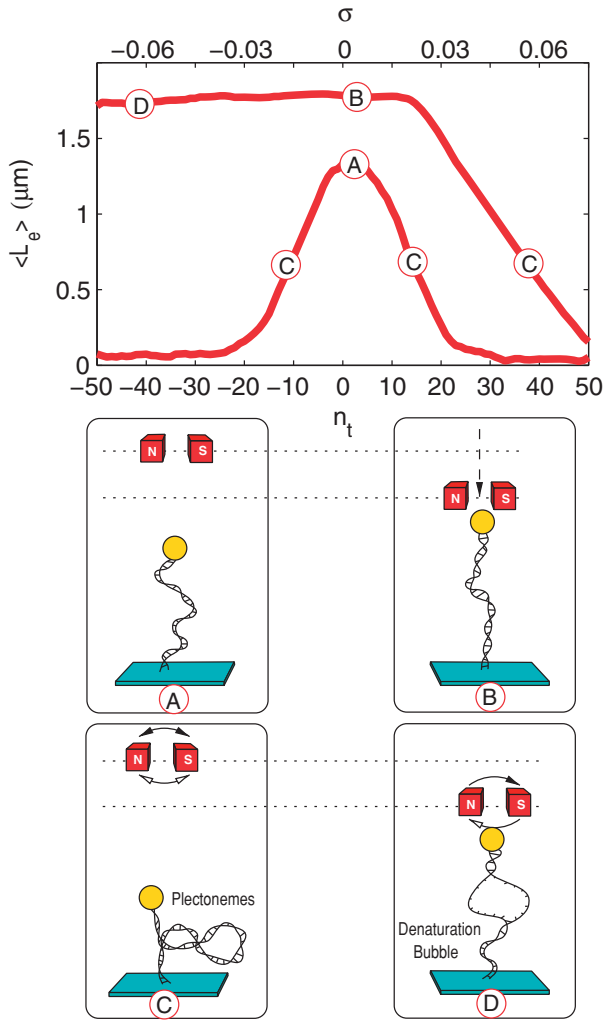

Figure 1. Upper panel: representative average DNA extension $\langle L_e \rangle$ measured using MT as a function of the number of imposed turns n_t (lower x axis) and of the degree of supercoiling σ (upper x axis). Data obtained in standard conditions (pH = 7.4, I_s = 150 mM) with F = 1.2 pN (upper data) and F = 0.45 pN (lower data). Lower panels A, B, C and D: schematic sketches of the DNA-magnetic bead arrangements during the MT experiments. The red circles over-plotted on the data highlight the correspondence between the schematic sketches and the DNA structures.

distribution of $\Delta L_e = (L_e - \langle L_e \rangle)$ for the data highlighted by the coloured circles. The histograms are fitted by Gaussian distributions, and the resulting values of the standard deviations σ_{L_e} for F = 0.8 pN and $n_t < -20$ (i.e. in the transition region between the plectonemic and denaturation states) seem to be larger with respect to other domains of F and n_t.

To explore this phenomenon quantitatively, we also calculated the temporal autocorrelation function $g(\tau) = \langle L_e(t) L_e(t+\tau) \rangle / \langle L_e(t)^2 \rangle$ for various values of the time delay τ. Two examples of the obtained correlation functions and the corresponding original data traces of the DNA extension versus time are presented in Figure 3, panel A and B, respectively. As apparent from Figure 3, the correlation function is negligible for F = 0.5 pN, that is, the correlation between the data occurs on a short time interval compared with our acquisition time.

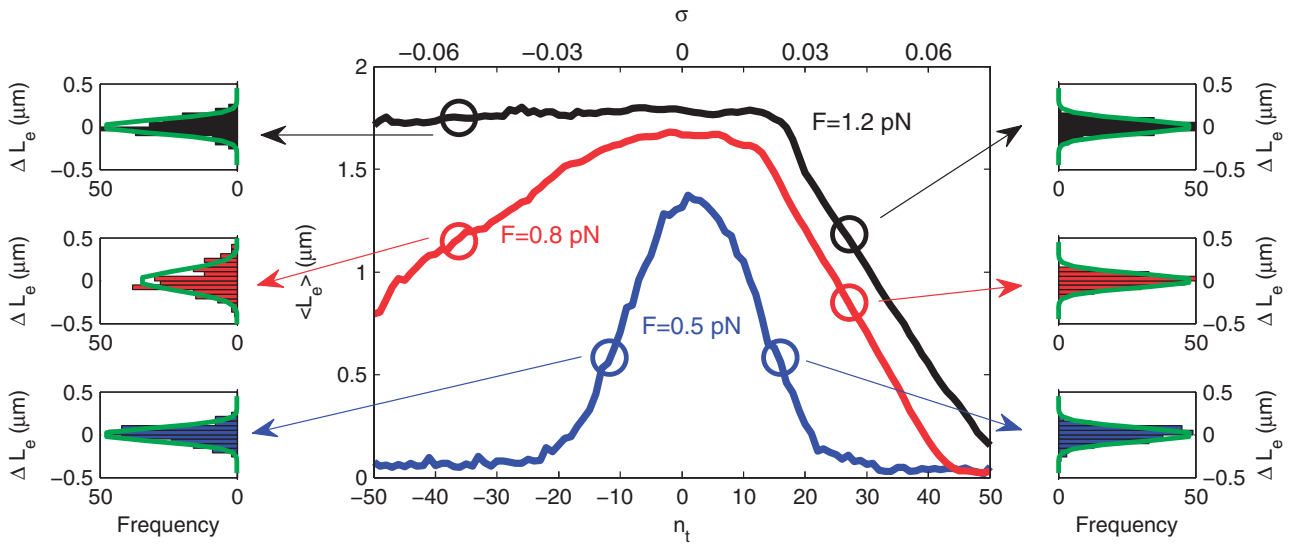

Figure 2. Average DNA extension $\langle L_e \rangle$ measured using the MT technique as a function of the number of imposed turns n_t (lower x axis) and of the degree of supercoiling σ (upper x axis) at the various forces F indicated by the labels. The lateral histograms represent the statistical distribution of $\Delta L_e = L_e - \langle L_e \rangle$ (in μm) of the data highlighted by the coloured circles. Data obtained in standard conditions.

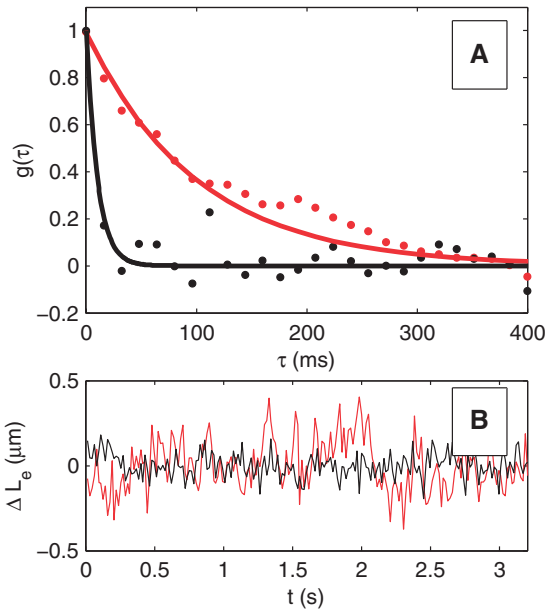

Figure 3. Panel A: normalized autocorrelation functions $g(\tau) = \langle L_e(t) L_e(t+\tau) \rangle / \langle L_e(t)^2 \rangle$ of the DNA extension fluctuations measured as a function of the delay time τ (symbols) and exponential fitting of the data (continuous line), which allows extracting the characteristic τ_{char}. Panel B: original temporal traces of the DNA extension fluctuations ΔL_e corresponding to the data of Panel A. Data obtained in standard conditions at $n_t = -40$ and $F = 0.5$ pN (black symbols) and 0.8 pN (red symbols).

For $F = 0.8$ pN, the correlation function is a decreasing function over an appreciable duration time of the order of 100 ms. We fitted the correlation functions with an exponentially decaying expression of the form $g(\tau) = e^{-\frac{\tau}{\tau_{char}}}$, where τ_{char} (the characteristic correlation time) is the free fitting parameter.

The data of the standard deviations obtained as a function of the number of imposed turns n_t and the applied forces F are presented in Figures 4A and 5A, respectively. Analogously, the measured τ_{char} values, as resulting from the previously described fitting procedure, are shown in Figures 4B and 5B for different values of the n_t and F. In Figure 4A and B, we have also showed the error bars as coloured bands around the data. Given the acquisition frame rate of the camera, we choose a value of 50 ms as a confidence threshold. The data below that threshold are not reliable. To emphasize this consideration, we have added to the figures showing τ_{char} a dashed horizontal line, indicating the limit of validity of the experimental fitting procedure for extracting τ_{char}.

It is worthwhile to note that to avoid systematic statistical errors, the values of σ_{L_e} and $\langle L_e \rangle$ are obtained by making a statistical average, that is, collecting data during a time interval of ∼100 of the corresponding τ_{char}. However, we have verified that the plotted values of σ_{L_e}, τ_{char} and $\langle L_e \rangle$ were not modified by increasing further the time interval of the statistical averaging. As clearly shown by Figures 4 and 5, the data seem to be more noisy and more correlated in a specific range of n_t and F. Indeed, the values of the standard deviation σ_{L_e} and τ_{char} below a fixed negative value of n_t ($n_t < -20$) are larger with respect to other domains of F and n_t. The values of σ_{Le} and τ_{char} show both a clear maximum around a characteristic value of the force ($F_{char} = 0.8$ pN). The value of F_{char} coincides for both σ_{L_e} and τ_{char}. The obtained F_{char} seems to not depend on n_t within the experimental errors, and the maximum values of σ_{Le} and τ_{char} at $F = F_{char}$, in the range explored, are decreasing functions of n_t.

The domains with large values of σ_{L_e} and τ_{char} are located in regions where, under the action of the imposed turns and forces, the DNA is fluctuating between the denaturated and plectonemic states, continuously exploring all the intermediate states. Because the possibility for DNA denaturation is strongly dependent

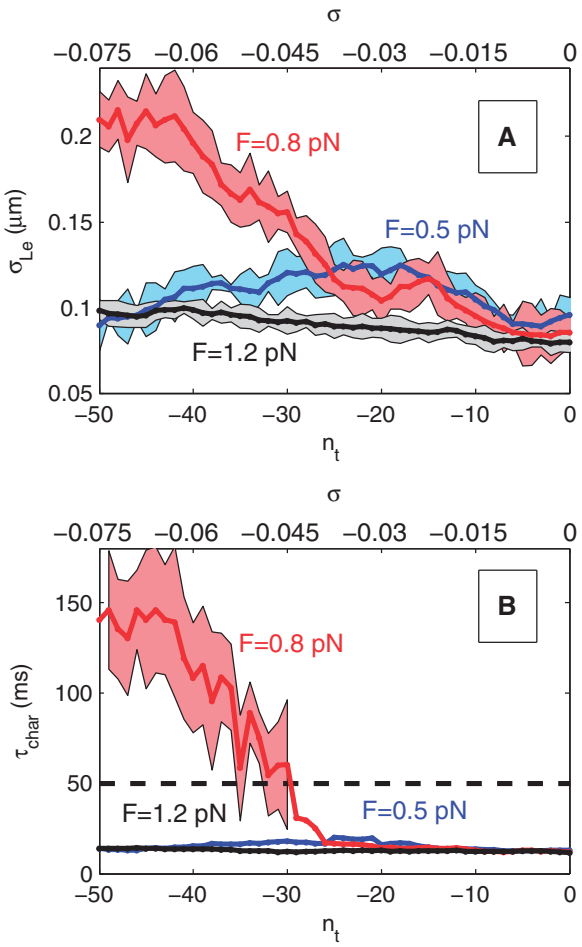

Figure 4. Standard deviation σ_{L_e} of the DNA extension (Panel A) and characteristic time τ_{char} of the correlation functions of the DNA extension fluctuations (Panel B) measured as a function of the number of imposed turns n_t (lower x axis) and of the degree of supercoiling σ (upper x axis). The horizontal dashed line represents the reliability threshold of the fitting procedure for obtaining τ_{char}, because of the finite acquisition time of the experiments. The coloured bands represent the error bars (confidence regions) as obtained by considering the quality of the fitting procedure. Data obtained in standard conditions at the different forces F indicated by the labels.

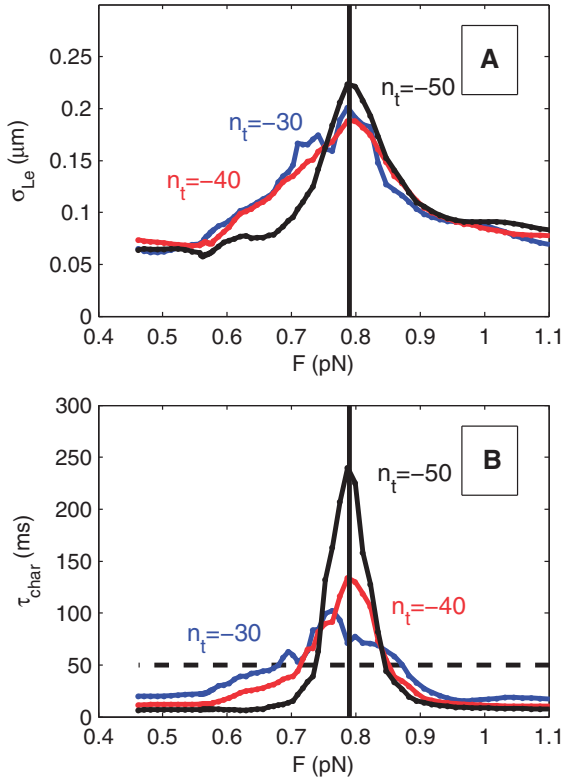

Figure 5. Standard deviation σ_{L_e} of the DNA extension (Panel A) and characteristic time τ_{char} of the correlation functions of the DNA extension fluctuations (Panel B) measured as a function of the force F. In all cases, the estimated errors are below the 20% of the measured values. The horizontal dashed line in Panel B represents the reliability threshold of the fitting procedure for obtaining τ_{char}, because of the finite acquisition time of the experiments. Data obtained in standard conditions at the different number of imposed turns n_t indicated by the labels. The vertical line indicates the characteristic force F_{char}.

on the acid–base or ionic characteristic of the solvent in which the DNA is dispersed (54), we have repeated the aforementioned analysis for different values of pH and I_s.

To investigate this point, we measured $\langle L_e \rangle$ versus n_t at fixed force for various values of pH and I_s, and the results are presented in Figure 6A and B, respectively. In this study, we directed our attention to the data at negative n_t, where a mild or flat dependence of $\langle L_e \rangle$ as a function of $|n_t|$ is a clear indication of the induced mechanical denaturation of the DNA molecule. As noticeably demonstrated in Figure 6A, the denaturation occurred more easily for pH values far from pH 7.4, where the hydrogen bonds of the bases are weaker (55). Similarly shown in Figure 6B, the DNA is easily denaturated for negative n_t at $I_s = 5$ mM, that is, at low ionic strength, where the screening of the electrostatic repulsion of the two double strands is reduced.

More quantitatively, in Figure 7A–D, we have plotted the extracted values of the standard deviations and the characteristic correlation times measured as a function of the applied F for different pH and I_s at negative imposed turn $n_t = -40$. From the entire ensemble of data, we extracted the values of the characteristic force in the different situations. The data show that at pH values other than pH 7.4 or for low ionic strength, the DNA transition to denaturation is shifted to lower values of F_{char}, that is, the DNA is less stable. By considering Figure 7, we can observe that the distribution of forces over which the DNA length fluctuations occur is systematically larger for high ionic strength (and less systematically for non-physiological pH). Indeed, the denaturation occurs at lower forces in acid or basic environments or at low ionic strength, as shown in Figure 8A and B, where the F_{char} values are plotted as functions of pH and I_s.

The observed bell-like shape of F_{char} versus pH and the increasing dependence of F_{char} versus I_s are notably similar to the classical dependences observed for the DNA melting temperature T_m as functions of pH and I_s. Indeed, in Figure 8C and D, for comparison we plotted the behaviour of T_m versus pH and I_s as classically reported in literature (56,57). The similarity between the

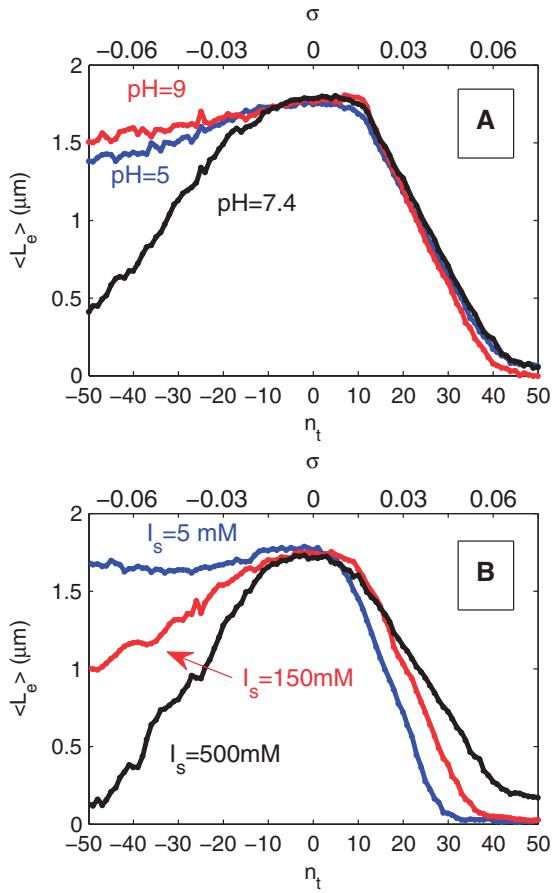

Figure 6. Average DNA extension $\langle L_e \rangle$ measured as a function of the number of imposed turns n_t (lower x axis) and of the degree of supercoiling σ (upper x axis). Data obtained at different pHs (see labels) with a constant force $F = 0.75$ pN and ionic strength $I_s = 150$ mM (Panel A). Data obtained at different ionic strengths I_s (see labels) with a constant force $F = 0.8$ pN and pH = 7.4 (Panel B).

behaviours confirms the capability of the method in characterizing the stability of DNA in different situations.

DISCUSSION

In the experimental results presented in this report, we mainly described the behaviour of DNA for negative imposed turns and for characteristic values of the applied force, where the DNA extension fluctuations are largely enhanced; the enhanced fluctuations are observed because molecules can choose between the mechanical options of locally denaturing (bubbles) or forming supercoils (plectonemes). We observed that such fluctuations are strongly dependent on the ionic strength and on the pH of the solvent.

We now recall the main results of a simplified quantitative model introduced in (40) which can describe all of the experimental findings. According to that model (40), when the DNA is twisted, the phenomenon of denaturation or plectoneme formation is accompanied by the stored energy $E_{tot} = E_{twist} + E_{plect} + E_{den} = \frac{1}{2}\frac{C}{L_0}(2\pi \cdot n_e)^2 + (2\pi R_p \cdot n_p) \cdot (\frac{B}{2R_p^2} + F) + \alpha \cdot n_d$. Where the first term is the twisting energy (E_{twist}), the second is the energy accumulated during plectoneme formation (E_{plect}) and the third one is the denaturating energy (E_{den}). L_0 is the extended length of the DNA, $n_e = (n_t - n_p - n_d)$ is the number of turns that store energy in the twist, n_p is the number of loops of radius R_p along the DNA, n_d is the number of turns relaxed by a partial DNA denaturation, B is the DNA bending constant, C is the DNA torsion constant and the constant α is proportional to the binding energy between the bases of the two DNA single strands. The first two terms were already used in model (6), whereas the last one was originally introduced in (40).

The plectonemic energy has a double origin: the work necessary for bending a $2\pi \cdot R_p$ portion of the double strand and the work for pulling the bead in presence of the force F. Disregarding the denaturation contribution, by minimizing the energy $E = E_{twist} + E_{plect}$, one can obtain the standard results of the equilibrium plectoneme radius $R_p = \sqrt{\frac{B}{2F}}$ and the buckling number $n_b = L_0 \frac{\sqrt{B \cdot F/2}}{\pi C}$, as previously reported in the literature (6).

The situation is more complicated when the denaturation contribution energy E_{den} is explicitly taken into account. The boundary conditions prescribe for E_{tot} a triangular validity region in the plane (n_p, n_d) with $n_t < n_p < 0$, $n_t < n_d < 0$ and $n_p + n_d < n_t$. The model (40) predicts the presence of a characteristic force F_{char}, where the energy necessary for relaxing a new turn by forming a loop or by denaturing the double strands is equal. The model analytically relates this characteristic force to the bending constant B and to the parameter α: $F_{char} = \frac{\alpha^2}{8B\pi^2}$.

The representative energy landscapes for three different values of the external force F are plotted in Figure 9A ($F < F_{char}$), Figure 9B ($F = F_{char}$) and Figure 9C ($F > F_{char}$) as a function of n_p and n_d. The darker regions in Figure 9A, B and C represent the equilibrium points or lines of minimum energy. The energy landscapes are obtained assuming standard values of $B = 50 \cdot k_B \cdot T$, $C = 140 \cdot k_B \cdot T$, $L_0 = 1.88$ μm and $\alpha = 1.12 \cdot 10^{-19}$ J. In the first case, when $F < F_{char}$, the energy landscape presents a minimum for $n_p = n_t - n_b$ (i.e. plectoneme formation) and $n_d = 0$ (i.e. no denaturation). In the case when $F > F_{char}$, the minimum of the energy is attained for $n_d = n_t - L_0 \cdot \alpha/(4C\pi^2)$ (i.e. the force is enough to form denaturation bubbles) and $n_p = 0$ (i.e. no formation of plectonemes). In the intermediate situation, when $F = F_{char}$, the minimum of the energy landscape is represented by a line, suggesting that the force is allowing a fluctuation along the line connecting the two states.

Using the experimental value $F_{char} \approx 0.8$ pN and a DNA persistence length of ∼50 nm, the resulting value of α is $\sim 1.1 \cdot 10^{-19}$ J ($\approx 66 kJ/mole$), which is approximately eight times the classically reported average value of the free energy per DNA base pair, $\Delta G \approx 8.4$ kJ/mole (58–60). It seems then necessary to open eight base pairs to relax one turn. This number of base pairs is consistent with the pitch of the double helix. This value is obtained not considering the influence of other possible structures [e.g. hairpin (61) or cruciform (62)]. The

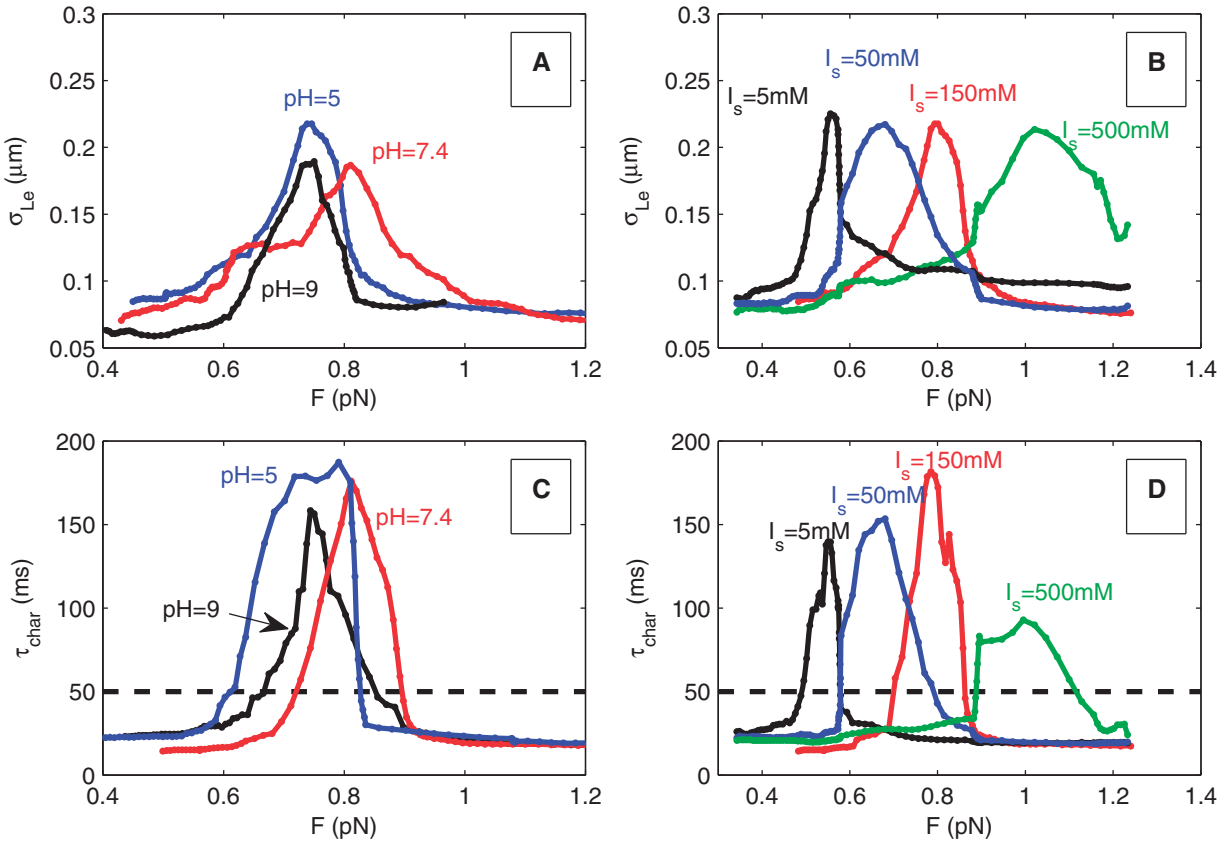

Figure 7. Standard deviation σ_{L_e} of the DNA extension (Panels A and B) and characteristic time τ_{char} of the correlation functions of the DNA extension fluctuations (Panels C and D) measured at the different values of pH (I_s = 150 mM) and ionic strengths (pH = 7.4) indicated by the labels. All data are acquired at negative imposed turn $n_t = -40$, and in all cases, the estimated errors are below the 20% of the measured values. The horizontal dashed line represents the reliability threshold of the fitting procedure for obtaining τ_{char}, because of the finite acquisition time of the experiments.

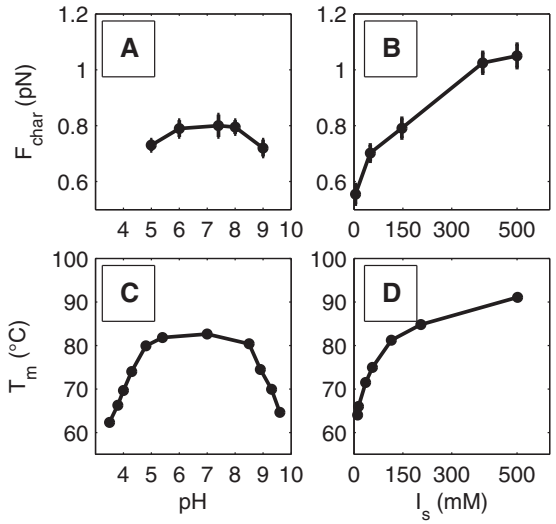

Figure 8. Characteristic force F_{char} measured as a function of the pH (Panel A) and of the ionic strength I_s (Panel B). Literature data (56,57) of the DNA melting temperature T_m measured as a function of the pH (Panel C) and of the ionic strength I_s (Panel D).

obtained value of α can be easily compared with the measured denaturation torque reported in (63). The parameter α is obtained by calculating the work necessary for twisting the DNA of one turn: $\alpha = \Gamma \cdot 2\pi$ (where Γ is the torque). By considering the reported torque of $11pN \cdot nm$, the calculated value for α is $0.7 \cdot 10^{-19} J$, consistent with what observed in the present work.

Using the proposed energy expression E_{tot} and a Boltzmann distribution enables a prediction for $\langle L_e \rangle$ and σ_{L_e} in the different situations. The calculated average DNA extension $\langle L_e \rangle$ is presented in Figure 9D as a function of n_t for three different force values. In this study, we suppose that the DNA extension variations are mainly because of plectoneme formation ($L_e = L_0 - 2\pi R \cdot n_p$). We also assume that the denaturation phenomenon does not introduced a significant DNA length variation given the low n_t values at which the experiments are performed. These n_t values correspond to a ssDNA of 300–350 bp, which is <5% of the DNA length. Evaluating the extension length of such ssDNA, and assuming 1 nm of persistence length, the maximum extension variation should be of the order of few 10th of nanometres, which is not relevant in our case. In the present calculations, we also introduced a worm-like chain model dependence of the extended value of the DNA length L_0 (64), and we also verified that the force dependence of the constant C is not strongly influencing the results (65). Comparing Figures 2 and 9D, we note that the model qualitatively describes not only the classical plectonemic behaviour observed for $n_t > 0$ but also the

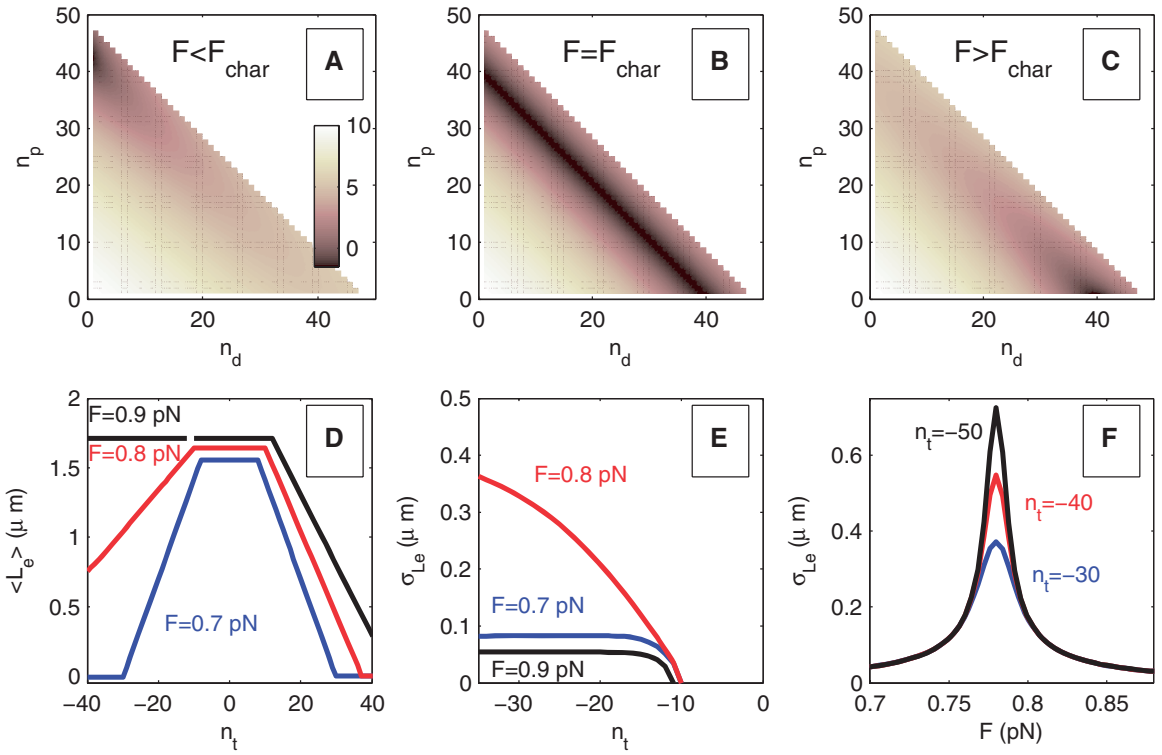

Figure 9. Contour plot of the theoretical energy landscape simulated as a function of the number of turns n_p relaxed in plectonemes and the number of denaturated turns n_d, calculated with the expression for E_{tot} described in the text, assuming 0.7 pN = $F < F_{char}$ (Panel A), 0.8 pN = $F = F_{char}$ (Panel B) and 0.9 pN = $F > F_{char}$ (Panel C). Intensity colour scale is expressed in terms of $k_B \cdot T$. Simulations obtained with the following parameters: $B = 50 \cdot k_B \cdot T$, $C = 140 \cdot k_B \cdot T$, $L_0 = 1.88\mu$m, $\alpha = 1.12 \cdot 10^{-19}$J. Panel D: calculated average DNA extension $\langle L_e \rangle$; Panels E and F: calculated standard deviations σ_{L_e} of the DNA fluctuations. Data calculated with the model described in the text as a function of the number of imposed turns n_t for the different values of the applied force F indicated in the labels.

transition between the plectonemic and denaturation regions for $n_t < 0$.

The qualitative agreement between the data and the model is also demonstrated by comparing the behaviour of the calculated σ_{L_e} as a function of n_t shown in Figure 9E and the experimental findings shown in Figure 4A. Both the calculated and measured fluctuations increase for $n_t < 0$ and in a specific range of F. The qualitative agreement is confirmed by Figures 9F and 5A, where we have shown the calculated and measured values of σ_{L_e} as a function of F. The similarity of the theoretical predictions and the data in all of the situations confirm the capability of the model to describe the characteristics of the experimental findings.

There are certain obvious quantitative differences between the measurements and the theory. For example, the calculated fluctuations show a transition from the plectonemic state towards the denaturating state in a narrow transition region of the force ($\pm 10\%$ of the F_{char}), whereas the experiments report a range larger ($\pm$ 20% of the F_{char}) than the model. This larger experimental fluctuation amplitudes with respect to the theoretical ones are presumably because of the fact that our model neglects several aspects of the real system, such as the presence of an initiation energy for starting the denaturation bubble (52), the possibility to have different bubbles along the DNA, the occurrence of different plectonemic regions (66) and the existence of thermal oscillations of the plectoneme radius (53). These considerations are also presumably the reason why the proposed model does not explain the observed dependence of the distribution of forces, over which the DNA fluctuations occur, on ionic strength or pH (Figure 7). In particular, an influence of the buffer condition on the number of plectoneme domains has been recently demonstrated (67). All these not considered ingredients can be at the origin of the quantitative differences between data and simulations. Nevertheless, the presented results reproduce qualitatively all the experimental conclusions, and the modelling can provide a deeper insight into the characteristics of DNA denaturation under the effects of external constraints. Other DNA structures (Z-DNA or L-DNA) can be formed at $n_t < 0$ (68–70), but all such structures are present in non-physiological conditions, far from the low force and turn regime, which is the object of the present work.

To consider the data taken in non-standard conditions of the solvent, we recall that the classical phenomenon of DNA denaturation that occurs at the temperature T_m depends on the specific DNA base composition and on environmental conditions (54). Indeed, at the temperature T_m, the hydrogen bonding between the bases weakens, and the two strands separate. T_m is a strongly dependent function of the pH and the ionic strength, as reported in the classical measurements (57,56) shown in Figure 8C and D.

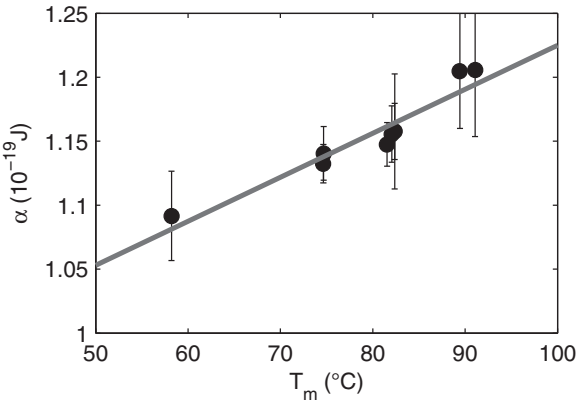

Figure 10. Symbols: measured denaturating parameter α plotted as a function of the melting temperature T_m obtained at different pH and ionic strengths I_s from the literature (56,57). Continuous line: linear fitting of the data. The error bars correspond to the distribution width of the α values obtained probing different molecules (~10).

We assume that the DNA melting occurs when the number of bases in the denaturation bubbles is comparable with half of the number of DNA base pairs. Considering a simplified version of the Poland–Scheraga model as reported in (71), the melting temperature T_m is related to the energy E_{el} for elongating a bubble by one base pair, by the relation $\frac{E_{el}}{k_B \cdot T_m} = 2 \cdot ln(2)$. Considering $E_{el} = \alpha/8$, where 8 is the number of base pairs opened to relax one loop, we predict a linear relationship between α and T_m with a theoretical proportionality constant m of $\sim 1.5 \cdot 10^{-22} J/^o K$. In Figure 10, the values of α, which are plotted as a function of the melting temperature measured at different pH and I_s, confirm this linear behaviour with a constant $m = 3.4 \pm 1 \cdot 10^{-22} J/^o K$. The order of magnitude agreement validates the appropriateness of the proposed model.

CONCLUSION

The data and the corresponding model shown in the present work elucidate new, innovative and fundamental aspects of DNA biophysics, specifically, the nanomechanical stability of single DNA molecules under various environmental conditions in a force and torsion regime compatible with those involved in important protein activities, such as DNA and RNA polymerases (72,73) and DNA gyrase (74). The presented research opens the way for further studies and investigations in more sophisticated and realistic situations; these studies could examine modified DNA structures or the effects of the presence of DNA binding proteins, enzymes and ligands.

ACKNOWLEDGEMENTS

S.E. acknowledges support from Regione Lombardia (Accordo per lo sviluppo del capitale umano nel sistema universitario lombardo). F. M. and D. S. wish to thank N. H. Dekker, D. Dulin and J. Lipfert for useful discussion about the magnetic tweezers data analysis. A.T. and V.C. acknowledge a profitable stay in Paris for the 2011 EMBO practical school organized by J.F. Allemand, K. Neuman and T. Strick. V.C. thanks B. Hommersom for the scientific discussions about the manuscript. All the authors thank the anonymous referees for their careful reading of the manuscript and their valuable suggestions.

FUNDING

Funding for open access charge: University of Milano-Bicocca.

Conflict of interest statement. None declared.

REFERENCES

1. Bustamante,C., Bryant,Z. and Smith,S.B. (2003) Ten years of tension: singlemolecule DNA mechanics. *Nature*, **421**, 423–427.
2. Ritort,F. (2006) Single-molecule experiments in biological physics: methods and applications. *J. Phys. Condes. Matter*, **18**, R531–583.
3. Neuman,K.C. and Nagy,A. (2008) Single-molecule force spectroscopy: optical tweezers, magnetic tweezers and atomic force microscopy. *Nat. Methods*, **5**, 491–505.
4. Strick,T.R., Allemand,J.F., Bensimon,D. and Croquette,V. (1998) Behavior of supercoiled DNA. *Biophys. J.*, **74**, 2016–2028.
5. Gosse,C. and Croquette,V. (2002) Magnetic tweezers: micromanipulation and force measurements at the molecular level. *Biophys. J.*, **82**, 3314–3329.
6. Strick,T.R., Dessinges,M.N., Charvin,G., Dekker,N.H., Allemand,J.F., Bensimon,D. and Croquette,V. (2003) Stretching of macromolecules and proteins. *Rep. Prog. Phys.*, **66**, 1–45.
7. Lipfert,J., Hao,X. and Dekker,N.H. (2009) Quantitative modeling and optimization of magnetic tweezers. *Biophys. J.*, **96**, 5040–5049.
8. te Velthuis,A.J.W., Kerssemakers,J.W.J., Lipfert,J. and Dekker,N.H. (2010) Quantitative guidelines for force calibration through spectral analysis of magnetic tweezers data. *Biophys. J.*, **99**, 1292–1302.
9. Dholakia,K., Spalding,G. and MacDonald,M. (2002) Optical tweezers: the next generation. *Phys. World*, **15**, 31–35.
10. Curtis,J.E., Koss,B.A. and Grier,D.G. (2002) Dynamic holographic optical tweezers. *Opt. Comm.*, **207**, 169–175.
11. Moffitt,J.R., Chemla,Y.R., Smith,S.B. and Bustamante,C. (2008) Recent advances in optical tweezers. *Annu. Rev. Biochem.*, **77**, 205–228.
12. Fazal,F.M. and Block,S.M. (2011) Optical tweezers study life under tension. *Nat. Photonics*, **5**, 318–321.
13. Lyubchenko,Y. and Shlyakhtenko,L.S. (1997) Visualization of supercoiled DNA with atomic force microscopy in situ. *Proc. Natl Acad. Sci. USA*, **94**, 496–501.
14. Rief,M., Clausen-Schaumann,H. and Gaub,H.E. (1999) Sequence-dependent mechanics of single DNA molecules. *Nat. Struct. Biol.*, **6**, 346–349.
15. Gómez-Navarro,C., Moreno-Herrero,F., dePablo,P.J., Colchero,J., Gómez-Herrero,J. and Baró,A.M. (2002) Contactless experiments on individual DNA molecules show no evidence for molecular wire behavior. *Proc. Natl Acad. Sci. USA*, **99**, 8484–8487.
16. Cassina,V., Seruggia,D., Beretta,G.L., Salerno,D., Brogioli,D., Manzini,S., Zunino,F. and Mantegazza,F. (2011) Atomic force microscopy study of DNA conformation in the presence of drugs. *Eur. Biophys. J. Biophys. Lett.*, **40**, 59–68.
17. Walter,N.G., Huang,C.Y., Manzo,A.J. and Sobhy,M.A. (2008) Do-it-yourself guide: how to use the modern single-molecule toolkit. *Nat. Methods*, **5**, 475–489.
18. Candelli,A., Wuite,G.J. and Peterman,E.J. (2011) Combining optical trapping, fluorescence microscopy and micro-fluidics for single molecule studies of DNA-protein interactions. *Phys. Chem. Chem. Phys.*, **13**, 7263–7272.
19. Dessinges,M.N., Maier,B., Zhang,Y., Peliti,M., Bensimon,D. and Croquette,V. (2002) Stretching single stranded DNA, a model polyelectrolyte. *Phys. Rev. Lett.*, **89**, 248102 1–5.

20. Mosconi,F., Allemand,J.F., Bensimon,D. and Croquette,V. (2009) Measurement of the torque on a single stretched and twisted DNA using magnetic tweezers. *Phys. Rev. Lett.*, **102**, 078301 1–4.
21. Deufel,C., Forth,S., Simmons,C.R., Dejgosha,S. and Wang,M.D. (2007) Nanofabricated quartz cylinders for angular trapping: DNA supercoiling torque detection. *Nat. Methods*, **4**, 223–225.
22. Celedon,A., Nodelman,I.M., Wildt,B., Dewan,R., Searson,P., Wirtz,D., Bowman,G.D. and Sun,S.X. (2009) Magnetic tweezers measurement of single molecule torque. *Nano Lett.*, **9**, 1720–1725.
23. Pedaci,F., Huang,Z., vanOene,M. and Dekker,N.H. (2012) Calibration of the optical torque wrench. *Opt. Express*, **20**, 3787–3802.
24. Mosconi,F., Allemand,J.F. and Croquette,V. (2011) Soft magnetic tweezers: A proof of principle. *Rev. Sci. Instrum.*, **82**, 034302 1–12.
25. Smith,S.B., Finzi,L. and Bustamante,C. (1992) Direct mechanical measurements of the elasticity of single DNA molecules by using magnetic beads. *Science*, **258**, 1122–1126.
26. Bustamante,C., Marko,J.F., Siggia,E.D. and Smith,S. (1994) Entropic elasticity of λ-phage DNA. *Science*, **265**, 1599–1600.
27. Strick,T.R., Allemand,J.F., Bensimon,D., Bensimon,A. and Croquette,V. (1996) The elasticity of a single supercoiled DNA molecule. *Science*, **271**, 1835–1837.
28. Allemand,J.F., Bensimon,D., Lavery,R. and Croquette,V. (1998) Stretched and overwound DNA forms a pauling-like structure with exposed bases. *Proc. Natl Acad. Sci. USA*, **95**, 14152–14157.
29. van Erp,T.S., Cuesta-Lopez,S., Hagmann,J.G. and Peyrard,M. (2005) Can one predict DNA transcription start sites by studying bubbles? *Phys. Rev. Lett.*, **95**, 218104 1–4.
30. Metzler,R., Ambjornsson,T., Hanke,A. and Fogedby,H.C. (2009) Single DNA denaturation and bubble dynamics. *J. Phys. Condens. Matter*, **21**, 034111 1–14.
31. Nisoli,C., Abraham,D., Lookman,T. and Saxena,A. (2010) Thermally induced local failures in quasi-one-dimensional systems: Collapse in carbon nanotubes and necking in nanowires and opening of bubbles in DNA. *Phys. Rev. Lett.*, **104**, 025503 1–4.
32. Nisoli,C. and Bishop,A.R. (2011) Thermomechanics of DNA: Theory of thermal stability under load. *Phys. Rev. Lett.*, **107**, 068102 1–4.
33. Theodorakopoulos,N. and Peyrard,M. (2012) Base pair openings and temperature dependence of DNA flexibility. *Phys. Rev. Lett.*, **108**, 078104 1–4.
34. Lee,O.C., Jeon,J.H. and Sung,W. (2010) How double-stranded DNA breathing enhances its flexibility and instability on short lenght scales. *Phys. Rev. E*, **81**, 021906 1–4.
35. Marko,J.F. (2007) Torque and dynamics of linking number relaxation in stretched supercoiled DNA. *Phys. Rev. E*, **76**, 021926 1–13.
36. Wildes,A., Theodorakopoulos,N., Valle-Orero,J., Cuesta-Lopez,S., Garden,J.L. and Peyrard,M. (2011) Thermal denaturation of DNA studied with neutron scattering. *Phys. Rev. Lett.*, **106**, 034302 1–4.
37. Kamashev,D., Balandina,A., Mazur,A.K., Arimondo,P.B. and Rouviere-Yaniv,J. (2008) Hu binds and folds single-stranded DNA. *Nucleic Acids Res.*, **36**, 1026–1036.
38. Geggier,S., Kotlyar,A. and Vologodskii,A. (2011) Temperature dependence of DNA persistence length. *Nucleic Acids Res.*, **39**, 1419–1426.
39. Martinez,I.A., Raj,S. and Petrov,D. (2012) Colored noise in the fluctuations of an extended DNA molecule detected by optical trapping. *Eur. Biophys. J. Biophys. Lett.*, **41**, 99–106.
40. Salerno,D., Tempestini,A., Mai,I., Brogioli,D., Ziano,R., Cassina,V. and Mantegazza,F. (2012) Single molecule study of the DNA denaturation phase transition in the force-torsion space. *Phys. Rev. Lett.*, **109**, 118303 1–5.
41. Salerno,D., Brogioli,D., Cassina,V., Turchi,D., Beretta,G.L., Seruggia,D., Ziano,R., Zunino,F. and Mantegazza,F. (2010) Magnetic tweezers measurements of the nanomechanical properties of DNA in the presence of drugs. *Nucleic Acids Res.*, **38**, 7089–7099.
42. Allemand,J.F., Bensimon,D., Jullien,L., Bensimon,A. and Croquette,V. (1997) pH-dependent specific binding and combing of DNA. *Biophys. J.*, **73**, 2064–2070.
43. Brogioli,D. *Design of magnetic tweezers for DNA manipulation.* , , http://arxiv.org/abs/0907.4601 (13 November 2012, date last accessed).
44. Lipfert,J., Klijnhout,S. and Dekker,N.H. (2010) Torsional sensing of smallmolecule binding using magnetic tweezers. *Nucleic Acids Res.*, **38**, 7122–7132.
45. Strick,T.R., Allemand,J.F., Bensimon,D., Bensimon,A. and Croquette,V. Apparatus and method for the manipulation and testing of molecules, and in particular of DNA. Pub. No.: US 2003/0027187 A1: [0052],[0053],[0054] February 2003 [0052],[0053],[0054].
46. Strick,T.R., Allemand,J.F., Bensimon,D., Bensimon,A. and Croquette,V. Apparatus and method for the manipulation and testing of molecules, and in particular of DNA. Pub. No.: US 2003/0166262 A1: [0052],[0053],[0054] September 2003 [0052],[0053],[0054].
47. Brogioli,D., Croccolo,F., Cassina,V., Salerno,D. and Mantegazza,F. (2008) Nano-particle characterization by using exposure time dependent spectrum and scattering in the near field methods: How to get fast dynamics with low-speed ccd camera. *Opt. Express*, **16**, 20272–20282.
48. Bouchiat,C., Wang,M., Allemand,J., Strick,T., Block,S. and Croquette,V. (1999) Estimating the persistence length of a worm-like chain molecule from force-extension measurements. *Biophys. J.*, **76**, 409–413.
49. Neukirch,S. (2004) Extracting DNA twist rigidity from experimental supercoiling data. *Phys. Rev. Lett.*, **93**, 198107 1–4.
50. Goyal,S., Perkins,N.C. and Lee,C.L. (2005) Nonlinear dynamics and loop formation in Kirchhoff rods with implications to the mechanics of DNA and cables. *J. Comp. Phys.*, **209**, 371–389.
51. Purohit,P.K. (2008) Plectoneme formation in twisted fluctuating rods. *J. Mech. Phys. Solids*, **56**, 1715–1729.
52. Forth,S., Deufel,C., Sheinin,M.Y., Daniels,B., Sethna,J.P. and Wang,M.D. (2008) Abrupt buckling transition observed during the plectoneme formation of individual DNA molecules. *Phys. Rev. Lett.*, **100**, 148301 1–4.
53. Brutzer,H., Luzzietti,N., Klaue,D. and Seidel,R. (2010) Energetics at the DNA supercoiling transition. *Biophys. J.*, **98**, 1267–1276.
54. Cantor,C.R. and Schimmel,P.R. (1980) *Biophysical Chemistry, Part III: The Behavior of Biological Macromolecules*. W. H. Freeman and Company, New York, NY, pp. 1157–1159.
55. Wood,J.L. (1974) ph-controlled hydrogen-bonding. *Biochem. J.*, **143**, 775–777.
56. Lando,D.Y., Haroutiunian,S.G., Kulba,A.M., Dalian,E.B., Orioli,P., Mangani,S. and Akhrem,A.A. (1994) Theoretical and experimental study of DNA helix-coil transition in acidic and alkaline medium. *J. Biomol. Struct. Dyn.*, **12**, 355–366.
57. Privalov,P.L., Ptitsyn,O.B. and Birshtein,T.M. (1969) Determination of stability of the DNA double helix in an aqueous medium. *Biopolymers*, **8**, 559–571.
58. Breslauer,K.J., Frank,R., Blocker,H. and Marky,L.A. (1986) Predicting DNA duplex stability from the base sequence. *Proc. Natl Acad. Sci. USA*, **83**, 3746–3750.
59. SantaLucia,J. (1998) A unified view of polymer and dumbbell, and oligonucleotide DNA nearest-neighbor thermodynamics. *Proc. Natl Acad. Sci. USA*, **95**, 1460–1465.
60. Owczarzy,R., Vallone,P.M., Gallo,F.J., Paner,T.M., Lane,M.J. and Benight,A.S. (1997) Predicting sequence-dependent melting stability of short duplex DNA oligomers. *Biopolymers*, **44**, 217–239.
61. Liphardt,J., Onoa,B., Smith,S.B., Tinoco,I.J. and Bustamante,C. (2001) Reversible unfolding of single RNA molecules by mechanical force. *Science*, **292**, 733–737.
62. Ramreddy,T., Sachidanandam,R. and Strick,T.R. (2011) Real-time detection of cruciform extrusion by single-molecule DNA nanomanipulation. *Nucleic Acids Res.*, **39**, 4275–4283.
63. Lipfert,J., Kerssemarkers,J.W., Jager,T. and Dekker,N.H. (2010) Magnetic torque tweezers: measuring torsional stiffness in DNA and RecA-DNA filaments. *Nat. Methods*, **7**, 977–980.
64. Marko,J.F. and Siggia,E.D. (1995) Statistical-mechanics of supercoiled DNA. *Phys. Rev. E*, **52**, 2912–2938.
65. Lipfert,J., Wiggin,M., Kerssemarkers,J.W., Pedaci,F. and Dekker,N.H. (2011) Freely orbiting magnetic tweezers to directly

monitor changes in the twist of nucleic acids. *Nat. Commun.*, **2**, 439 1–9.
66. Marko,J.F. and Neukirch,S. (2012) Competition between curls and plectonemes near the buckling transition of stretched supercoiled DNA. *Phys. Rev. E*, **85**, 011908 1–19.
67. vanLoenhout,M.T., deGrunt,M.V. and Dekker,C. (2012) Dynamics of DNA supercoils. *Science*, **338**, 94–97.
68. Sarkar,A., Leger,J.F., Chatenay,D. and Marko,J.F. (2001) Structural transitions in DNA driven by external force and torque. *Phys. Rev. E*, **63**, 051903 1–10.
69. Kouzine,F. and Levens,D. (2007) Supercoil-driven DNA structures regulate genetic transactions. *Front. Biosci.*, **12**, 4409–4423.
70. Sheinin,M.Y., Forth,S., Marko,J.F. and Wang,M.D. (2011) Underwound DNA under tension: structure, elasticity, and sequence-dependent behaviors. *Phys. Rev. Lett.*, **107**, 108102 1–5.
71. Philips,R., Kondev,J. and Theriot,J. (2009) *Physical Biology of the Cell*. Garland Science, San Diego, CA, pp. 308–310.
72. Davenport,R.J., Wuite,G.J., Landick,R. and Bustamante,C. (2000) Single-molecule study of transcriptional pausing and arrest by e.coli RNA polymerase. *Science*, **287**, 2497–2500.
73. Wuite,G., Smith,S.B., Young,M., Keller,D. and Bustamante,C. (2000) Single-molecule studies of the effect of template tension on t7 DNA polymerase activity. *Nature*, **404**, 103–106.
74. Nollmann,M., Stone,M.D., Bryant,Z., Gore,J., Crisona,N.J., Hong,S.C., Mitelheiser,S., Maxwell,A., Bustamante,C. and Cozzarelli,N.R. (2007) Multiple modes of Escherichia Coli DNA gyrase activity revealed by force and torque. *Nat. Struct. Mol. Biol.*, **14**, 264–271.